

# One-shot Visual Reasoning on RPMs with an Application to Video Frame Prediction

Wentao He, *Student Member, IEEE*, Jianfeng Ren, *Member, IEEE*, Ruibin Bai, *Senior Member, IEEE*

**Abstract**—Raven’s Progressive Matrices (RPMs) are frequently used in evaluating human’s visual reasoning ability. Researchers have made considerable effort in developing a system which could automatically solve the RPM problem, often through a black-box end-to-end Convolutional Neural Network (CNN) for both visual recognition and logical reasoning tasks. Towards the objective of developing a highly explainable solution, we propose a One-shot Human-Understandable ReaSoner (Os-HURS), which is a two-step framework including a perception module and a reasoning module, to tackle the challenges of real-world visual recognition and subsequent logical reasoning tasks, respectively. For the reasoning module, we propose a “2+1” formulation that can be better understood by humans and significantly reduces the model complexity. As a result, a precise reasoning rule can be deduced from one RPM sample only, which is not feasible for existing solution methods. The proposed reasoning module is also capable of yielding a set of reasoning rules, precisely modeling the human knowledge in solving the RPM problem. To validate the proposed method on real-world applications, an RPM-like One-shot Frame-prediction (ROF) dataset is constructed, where visual reasoning is conducted on RPMs constructed using real-world video frames instead of synthetic images. Experimental results on various RPM-like datasets demonstrate that the proposed Os-HURS achieves a significant and consistent performance gain compared with the state-of-the-art models.

**Index Terms**—Raven’s progressive matrices (RPM), RAVEN, visual reasoning, frame prediction

## I. INTRODUCTION

COMPUTER vision has recently achieved great advancements in many applications [1]–[6]. The research focus has gradually shifted from visual recognition of individual objects to visual understanding of scene images/videos. Visual reasoning [7] is one of the image-understanding tasks, which usually consists of two parts: “visual” and “reasoning”. The former relates to a visual system to gain information through vision ability [1], [3], [4], and the latter links to a cognitive system, focusing on using logic to discover rules and solve problems [8]–[13]. Significant research efforts are needed to develop a visual reasoning system that has not only the visual recognition capability, but also the capability of understanding image/video scenes and conducting logical reasoning based on the perceived image/video contents.

Visual reasoning in general can be categorized as: video action recognition [15]–[17], image/video captioning [18]–[20], visual question answering (VQA) [21]–[24], and visual IQ tests [10], [11]. The first two focus more on visual recognition

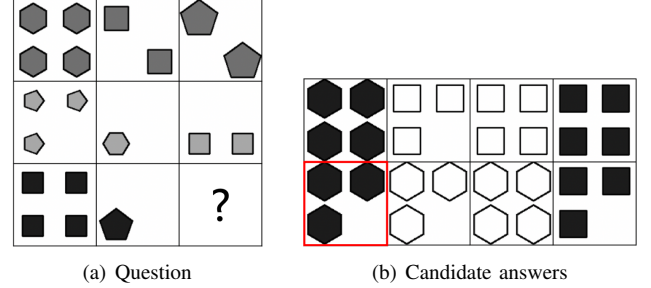


Figure 1. An example of the I-RAVEN dataset [14]. The correct answer is marked in red. The reasoning rules are deduced row-wisely based on the extracted visual attributes, i.e. *Arithmetic* (subtraction) on *Number*, *Distribute\_Three* on *Type*, *Progression* on *Size* and *Constant* on *Color*.

whereas the last two focus more on logical reasoning. Early models for action recognition and VQA develop reasoning abilities by building task-specific multilayer perceptrons or fine-tuning visual recognition models [25]. With the development of Relation Networks [8] and Graph Neural Networks [26], models with better reasoning abilities have been developed, but mostly for simple reasoning logic [26]–[28].

Logical reasoning consists of three taxonomies of reasoning, i.e., induction, deduction and abduction [29], [30]. Generic logical reasoning contains a premise (precondition), a conclusion (logical consequence) and a rule (material conditional) that implies the conclusion given the premise. Reasoning on complex image scenes is tremendously difficult [7], and hence very often the visual task is either simplified, e.g. Sort-of-CLEVR [8], [9] and Pretty-CLEVR [12], or the visual information is assumed available in advance [8], [12], [13]. One test frequently used on human’s visual reasoning ability in cognitive science is Raven’s Progressive Matrices (RPM) [31], [32]. Researches into solving RPM automatically can help to assess and improve the reasoning ability of computer vision systems. In literature, RPMs are often referred as abstract reasoning [11], [14], [33] or analogical reasoning [10], [32], [34], [35], and both of which enable a form of inductive reasoning [30]. An RPM problem is usually formed by a  $3 \times 3$  pictorial matrix with the last one left blank. The task is to infer the underlying rules from the given matrix and identify the missing entry from the list of given candidates. Fig. 1 shows an example of RPM problems.

Researchers have made considerable efforts in developing a system to automatically solve the RPM problem [33], [35]–[37]. Existing approaches often offer a black-box solution, which is difficult to be comprehended by humans and extendable to real-world problems. 1) Most existing solutions

utilize end-to-end CNNs [14], [33]–[38]. Such a network may not be able to handle the tremendous combinations of complex visual recognition tasks and diversified logical reasoning tasks. 2) Most existing methods [14], [33]–[38] aim to discover the underlying reasoning rule that directly maps from eight problem images to one of the candidate answers. Such “8+1” formulation neglects the fact that humans often solve RPM-like problems row-wisely or column-wisely. As shown later in Section III-C, this formulation greatly enlarges the input to the system and unnecessarily complicates the model. 3) Due to the “8+1” formulation, it is difficult or even impossible to extract any logical reasoning rules that could be understood by humans. The human-understandable reasoning rules in RPM-like problems are overwhelmed in the existing black-box solutions [14], [33]–[38].

To address these problems, we propose a solution simulating human’s visual reasoning process, named as One-shot Human-Understandable ReaSoner (Os-HURS). 1) To handle complex and diversified visual reasoning tasks, instead of an end-to-end network, we propose a two-stage visual reasoning framework. The first stage, a perception module, aims to visually understand the image scenes and generate human-understandable visual attributes. The second stage, a reasoning module, aims to build human-understandable reasoning rules based on the derived visual attributes. This two-stage design could make good use of existing developments in both computer vision and logical reasoning societies, and well handle the complicated and diversified real-world visual reasoning tasks. 2) In contrast to the existing “8+1” formulation [14], [33]–[38], we formulate the problem as three groups of “2+1” image sets for each problem panel row-wisely, i.e. based on the first two images, the target is to derive the underlying rules that define the third image, and the rules should be consistent across three groups. This is very close to human’s reasoning process. As illustrated later in Section III-C, the proposed “2+1” formulation leads to a more efficient and elegant solution to the RPM problem. A precise reasoning rule could be deduced from just one RPM sample by utilizing the proposed formulation, which is not feasible for the existing “8+1” formulation. 3) Beneficial from the proposed “2+1” formulation, the proposed approach could produce a set of reasoning rules that can be translated to human-understandable rules. More specifically, we show that we can model most of the human-understandable reasoning rules efficiently and precisely using the proposed method, as illustrated later in Section III-D.

Due to the complicated network structure of deep learning algorithms, the machine decisions from these networks are difficult for humans to understand [39]. However, a wide range of fields and disciplines requires a high level of interpretability, reliability and trustworthiness for artificial intelligence methods, particularly in medical sector [39], manufacturing [40] and cognitive science [41]. The human-understandable explanations of machine decisions brought by explainable artificial intelligence (XAI) is essential to justify the reliability of AI models, which allows human users to comprehend and trust the output results created by the “white-box” machine learning algorithms [42].

RPM problems represent a category of challenging visual

reasoning problems, one-shot visual reasoning problem, e.g., given the first two rows (each with three images) only, a set of consistent rules need to be discovered from images and applied to the third row to find the last missing image. Although RPM problems are artificially generated, they have been used to evaluate the reasoning ability of humans and various visual reasoning models [14], [33]–[38]. To evaluate the proposed method in real-world applications, we construct an RPM-like One-shot Frame-prediction (ROF) dataset. The artificially generated images in RPMs are replaced by the video frames of the UA-DETRAC dataset [43], a benchmark real-world multi-object detection and tracking dataset. The target here is to predict the future frame given the two previous frames at intervals of time, together with the first two frame triplets from other videos. To simplify the task, eight candidate answers are provided. The problem is formulated under the RPM framework to assess the visual reasoning capability of the proposed method and many other models. More details can be found in Section IV.

The proposed approach is compared with state-of-the-art methods such as CoPINet [36] and SRAN [14] on the two widely used benchmark datasets, RAVEN [10] and I-RAVEN [14], their shrunk versions and the developed ROF dataset to evaluate the reasoning capability of models. The proposed method significantly improves the average visual reasoning accuracy from 91.4% to 93.1% compared with the previously published best results by CoPINet [36] on the RAVEN dataset, and from 60.8% to 95.9% compared with the previously published best result by SRAN [14] on the I-RAVEN dataset. On the ROF dataset, the proposed method outperforms CoPINet [36] by 9.24% and SRAN [14] by 7.69%.

Our contributions are summarized as follow: 1) We propose a one-shot two-step framework making good use of developments in both computer vision and logical reasoning societies and solving the RPM problem in a highly explainable way. 2) The proposed “2+1” formulation generates a precise reasoning rule by utilizing one sample question only, which greatly simplifies the model and yields an elegant and efficient solution. 3) Thanks to the two-step framework and “2+1” formulation, the proposed solution could yield a set of reasoning rules adaptive to various scenarios covering almost all human-understandable reasoning rules in RPM-like problems. 4) We develop a benchmark RPM-like One-shot Frame-prediction dataset and successfully apply the proposed method to solve the complicated real-world visual reasoning problems.

## II. RELATED WORKS

### A. Visual Reasoning

Image/video understanding has been studied for decades, while visual reasoning only recently attracted the attention of researchers. It first visually recognizes the attributes from image/video scenes [2], [5] and then conducts relational reasoning based on the derived attributes [8]–[13]. Visual reasoning requires efforts from both computer science and cognitive science, and develops linkages between recognition and cognition [7]. In literature, visual reasoning spans a variety of tasks, e.g., video action recognition [15]–[17], image/video

captioning [18]–[20], visual question answering [21]–[24], [44]–[46], and Raven’s Progressive Matrices [14], [32]–[38].

Activity recognition highly relies on temporal information. To efficiently recognize actions in video sequences, reasoning about human-object relations over time becomes a crucial challenge [16]. Wang *et al.* [15] introduced Temporal Segment Network based on BN-Inception architecture. Zhou *et al.* [16] improved it by utilizing Temporal Relation Network to focus on relational reasoning and learning temporal dependencies between video frames at multiple time scales.

Image/video captioning from a relation-reasoning perspective has recently received an increasing attention [47]. Yao *et al.* [20] developed an image captioning scheme based on semantic and spatial object relationships, with a relation-aware region representation derived by Graph Convolutional Network, which generates captions by utilizing the region-level attention mechanism of LSTM. Hou *et al.* [47] built models exploiting relationships between scene objects and prior knowledge for image and video captioning.

Visual question answering (VQA) is a conventional visual reasoning task that measures the machine understanding of scene-level images. The objective is to derive an accurate natural language answer, given an image and a related natural language question [21]. Early VQA tasks are based on natural scene images [21], [24], [48]. Johnson *et al.* [22] developed the CLEVR dataset by replacing natural images with synthetic images to address the challenge of complicated background in natural images. Wang *et al.* [23] developed the fact-based VQA that contains supportive natural language facts to assist reasoning. Recently, a new form of VQA tasks was developed by Zellers *et al.* as Visual Commonsense Reasoning [7], whose objective is to answer the question and/or provide an explanation why the answer is correct.

### B. Raven’s Progressive Matrices

Raven’s Progressive Matrices (RPMs) are originally designed as a non-verbal assessment for human intelligence. By using pictorial matrices containing visually simple patterns, it minimizes the impact of language barrier and culture bias. Recently, large-scale RPM-style datasets, RAVEN [10] and its variants [14], were introduced to extend the RPM-related study from cognitive science to computer science. The RPM-style datasets [10], [14] are often automatically generated, and the problems are solved with minimal prior knowledge about the internal construction rules.

Santoro *et al.* [11] developed a reasoning algorithm called Wild Relation Network (WRen), which applies a Relation Network to model the relationship between the question panel and the candidate answer. Zhang *et al.* [10] developed a ResNet architecture assembled with a Dynamic Residual Tree (DRT) module for reasoning [10]. They later developed an improved network architecture called CoPINet [36] under the principle of contrasting, which achieved the previous best performance on the RAVEN dataset. Hu *et al.* [14] argued that RAVEN has a shortcut to solutions, and hence developed an I-RAVEN dataset balancing the candidate answer sets and the solution model. Their developed solution model, SRAN [14], achieves the state-of-the-art results on the I-RAVEN dataset.

Various models have been developed in literature to solve the RPM-like problems [14], [33]–[35], [37], [38]. However, most of them are based on the black-box CNN models not understandable by humans, whereas the RPM-like problems are originally designed to evaluate human intelligence and mostly solvable by humans. In this paper, we propose a highly explainable framework simulating human’s reasoning process, which outperforms all the existing RPM solvers.

### C. Video Frame Prediction

Video prediction is an emerging research field of computer vision [49]–[51]. It has been successfully applied in various applications such as action anticipation [52], prediction of object locations [53], trajectory prediction [54], anomaly detection [55] and many more. Given a sequence of previous frames, the target of video prediction is to reason and predict about the subsequent frame(s) based on the analysis of rich spatio-temporal features in a video, e.g., object/background information or regularity of pixel changes [51].

In literature, many solution models such as convolutional models, recurrent models and generative models have been designed to tackle the video prediction problem [56]–[58]. Most of the models can be classified into four main categories, direct pixel synthesis, factoring the prediction space, narrowing the prediction space and incorporating uncertainty [51]. For instance, Jin *et al.* [59] developed a generative adversarial network to synthesize future frames based on multi-level wavelet analysis, given a set of previous frames. To reduce the prediction space, Villegas *et al.* [60] extracted the human pose as an additional supervision signal, and regressed future frames through analogy making. Recently, Chen *et al.* [49] predicted motions of different key objects to generate sharper and more realistic frame predictions. For a more comprehensive review on video prediction, readers are referred to [51].

## III. REASONING ON RAVEN’S PROGRESSIVE MATRICES

### A. Proposed Two-step Framework

Formally, in a  $3 \times 3$  RPM-like problem, the query image matrix  $\mathbf{I}^q$  and the candidate answer set  $\mathbf{I}^c$  can be represented as:

$$\mathbf{I}^q = \begin{bmatrix} I_{1,1}^q & I_{1,2}^q & I_{1,3}^q \\ I_{2,1}^q & I_{2,2}^q & I_{2,3}^q \\ I_{3,1}^q & I_{3,2}^q & I_{3,3}^q \end{bmatrix}, \quad (1)$$

$$\mathbf{I}^c = \{I_1^c, I_2^c, \dots, I_8^c\}, \quad (2)$$

where the last missing image  $I_{3,3}^q$  is filled by the ground-truth answer  $I_*^c$  from the candidate answer set  $\mathbf{I}^c$ , as shown in Fig. 1. A set of questions with known correct candidate answers serve as training samples  $\langle \mathbf{I}_{(i)}^q, \mathbf{I}_{(i)}^c \rangle, i = 1, \dots, n$ , where  $n$  is the size of the training set. The objective is to identify the correct candidate image  $I_*^c$  from  $\mathbf{I}^c$  based on the

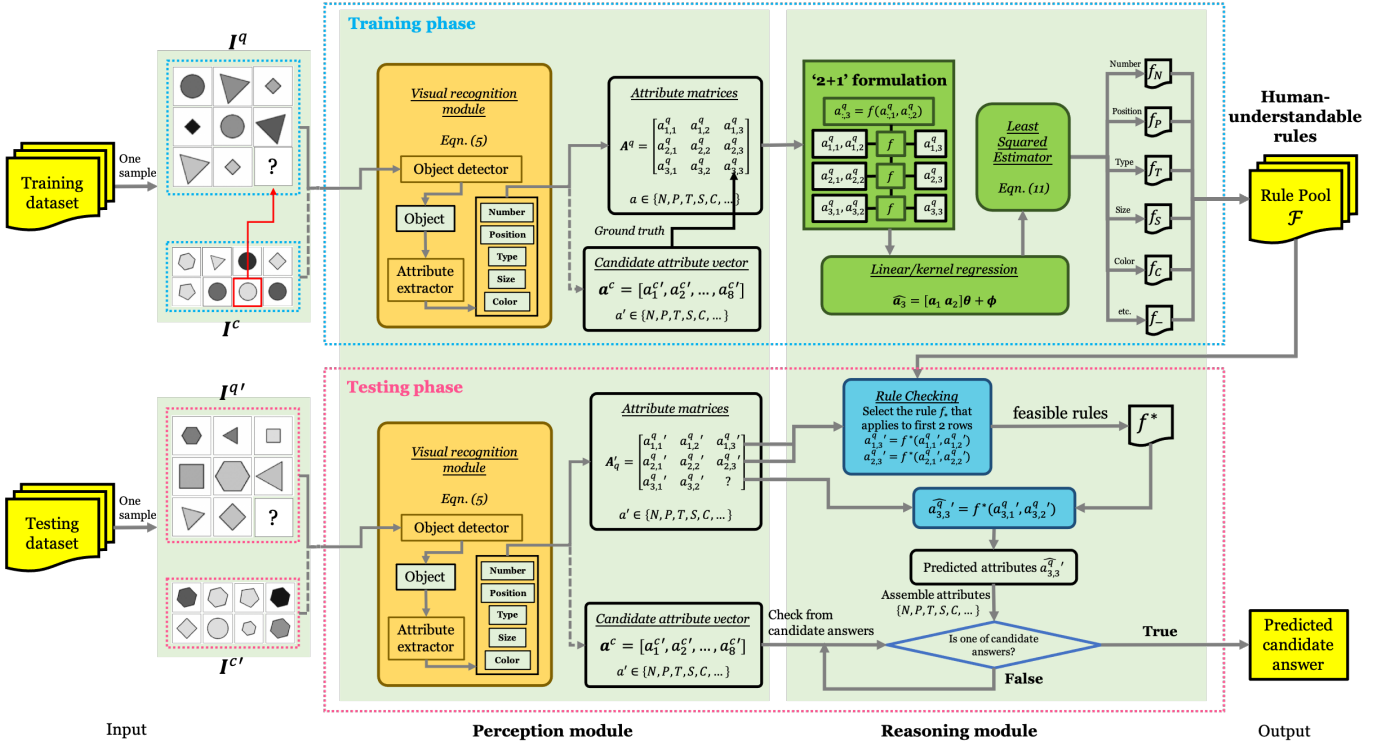


Figure 2. Block diagram of the proposed RPM solver. The visual attributes are first derived by the perception module, and used to extract the reasoning rules by the reasoning module. By utilizing the proposed “2+1” formulation, a precise reasoning rule can be extracted by a least-squares estimator as in Eqn. (10) for each attribute using one sample problem only. During testing, the visual attributes of a testing sample are first derived by the perception module and then evaluated against the rules in the rule pool  $\mathcal{F}$  using Eqn. (8). The proposed method yields an efficient and elegant solution model that can be easily understood by humans.

derived attribute matrix  $A^q$  and the candidate attribute vector  $a^c$ , together with the underlying reasoning rule  $f$ :

$$A^q = \begin{bmatrix} a_{1,1}^q & a_{1,2}^q & a_{1,3}^q \\ a_{2,1}^q & a_{2,2}^q & a_{2,3}^q \\ a_{3,1}^q & a_{3,2}^q & a_{3,3}^q \end{bmatrix}, \quad (3)$$

$$a^c = \{a_1^c, a_2^c, \dots, a_8^c\}, \quad (4)$$

where visual attributes  $a^q, a^c \in \{N, P, T, S, C\}$  are either the attributes of *Number*, *Position*, *Type*, *Size* or *Color* of a question/candidate image, which will be deduced through the perception module.

For humans, the problems are usually solved in two steps: the visual attributes are first derived from input images through the visual perception system, and then reasoning rules are deduced based on the derived visual attributes through the logical reasoning system. When solving RPMs, humans may try a series of logical reasoning rules generated by human’s cognition system, and apply the most appropriate one to predict the correct answer.

For most existing methods, visual recognition and logic reasoning are assembled into one CNN architecture [14], [33]–[38]. Such techniques may sound technically appealing and may work in a situation where either visual recognition or logical reasoning is relatively easy. However, often in visual reasoning, the image scenes are so complicated [15]–[20] that a dedicated system is needed to accomplish a specific visual

recognition task, and many different systems of such types are needed for various tasks. In addition, the reasoning modules would be different for different reasoning tasks. Therefore, it is extremely difficult to build an end-to-end architecture that could work well for various visual reasoning tasks.

In contrast, the proposed Os-HURS solves the visual reasoning problems by utilizing two separate modules, the perception module and the reasoning module. The former aims to address the challenges of deriving the visual attributes from the image/video, and the latter aims to tackle the challenges of deriving the logical reasoning rules based on the perceived visual attributes. By disassembling the whole framework into two modules, we could make good use of the recent developments in both visual recognition and logic reasoning to better solve the visual reasoning tasks.

**Training phase** The proposed framework consists of two stages: perception and reasoning. The objective of the first stage is to develop the perception module  $M_P$  that transfers the input images  $I^q$  and  $I^c$  into the set of visual attributes  $A^q$  and  $a^c$  later to be fed into the reasoning module  $M_R$ . More information on the perception module can be found in Section III-B. The objective of the second stage is to develop the reasoning module  $M_R$  that infers a set of reasoning rules based on the derived visual attributes  $A^q$  and  $a^c$  using the proposed “2+1” formulation. More specifically, for each row, given the visual attributes of the first two images, the target is to find the underlying rule  $f$  to derive the attributes of the third image. Compared to the “8+1” formulation used in existing



methods, the proposed “2+1” formulation greatly simplifies the model and leads to an elegant solution model, i.e. a precise reasoning rule could be deduced for each attribute using one sample question only. These reasoning rules then form the pool of reasoning rules  $\mathcal{F}$ , to be later used in testing. More details on logical reasoning can be found in Section III-C.

**Testing phase** During testing, given an image matrix  $I^{q'}$  and candidate image set  $I^{c'}$ , their corresponding visual attributes  $A^{q'}$  and  $a^{c'}$  are first derived using the proposed perception module  $M_P$ . At the reasoning stage, following the proposed “2+1” formulation, the target is to find a consistent rule  $f^*$  from the rule pool  $\mathcal{F}$  to apply on the first two rows. Note that more than one feasible rule  $f^*$  may be found at this point. Then all the feasible rules are applied on the third row to predict the correct candidate answer. If the predicted answer matches any candidate answer, it is treated as the final answer.

The proposed two-step framework for visual reasoning is consistent to human’s visual reasoning. It addresses the challenges of poor interpretability of existing end-to-end networks for visual reasoning. Moreover, complicated visual reasoning tasks involving complex visual recognition and diversified logical reasoning rules are potentially better solved in two steps rather than using one end-to-end network, as indicated later in the experiments.

### B. Perception Module

The aim of the perception module  $M_P$  is to extract the visual attributes  $a^q, a^c$  from the question image  $I^q$  or the candidate image  $I^c$ , i.e.

$$\begin{aligned} a^q &= M_P(I^q), \\ a^c &= M_P(I^c). \end{aligned} \quad (5)$$

In literature, many existing solutions can be used to derive these attributes [1], [3], [4]. In this paper, computationally efficient methods are utilized to extract the visual attributes from the images. The *Type* and *Size* attributes are determined using template matching [61]. The *Number* and *Position* attributes are derived through Connected Component Analysis, and the *Color* attribute are derived as the median intensity value of the polygon.

The derived perception module is utilized in both training and test phases to derive the visual attributes  $A^q$  for the input image matrix and  $a^c$  for the candidate images. The derived attributes have different meanings and should be handled differently with care. Attribute *Number*, *Type*, *Size* and *Color* are formed by a set of ordered values. For attribute *Position*, its values indicate whether there is an object at the corresponding position, e.g. for one  $2 \times 2$  image sub-patch with *Position* vector  $[1,0,0,1]$ , 1 indicates that there is an object and 0 otherwise. For all visual attributes, the categorical attribute values are transformed into numerical values.

The developed perception module perfectly recognizes all the attributes, *Type*, *Number/Position*, *Size*, *Color*, with an accuracy of 100%. The derived visual attributes are then fed into the reasoning module to discover the underlying rules governing the sample question.

### C. Reasoning Module using Proposed “2+1” Formulation

Traditionally, human solves RPM problems by finding a common rule  $R_H$  that simultaneously applies to all three rows,

$$a_{i,3}^q = R_H(a_{i,1}^q, a_{i,2}^q), \quad (6)$$

where  $a_{i,1}^q, a_{i,2}^q, a_{i,3}^q$  represent 3 attribute values of images in the  $i^{\text{th}}$  row. Following human’s reasoning process, we propose the “2+1” formulation. We redefine the  $3 \times 3$  attribute matrix  $A^q$  as follows:

$$\begin{aligned} A^q &= [a_1^q \ a_2^q \ a_3^q], \\ A_{1,2}^q &= [a_1^q \ a_2^q], \\ \text{where } a_1^q &= \begin{bmatrix} a_{1,1}^q \\ a_{2,1}^q \\ a_{3,1}^q \end{bmatrix}, a_2^q = \begin{bmatrix} a_{1,2}^q \\ a_{2,2}^q \\ a_{3,2}^q \end{bmatrix} \text{ and } a_3^q = \begin{bmatrix} a_{1,3}^q \\ a_{2,3}^q \\ a_{3,3}^q \end{bmatrix}. \end{aligned} \quad (7)$$

The RPM problems is transferred into a small-scale regression problem, i.e. for each question panel, given the input matrix  $A_{1,2}^q$ , the objective is to derive a regression rule  $f(\cdot)$  so that  $\hat{a}_3^q = f(A_{1,2}^q)$ , and the difference between  $\hat{a}_3^q$  and  $a_3^q$  should be minimized.

Our hypothesis starts with linear regression, as the reasoning rules defined in [10] are mainly unary operations, i.e.

$$\hat{a}_3^q = f(A_{1,2}^q) = A_{1,2}^q \theta + \phi, \quad (8)$$

where  $\theta \in \mathbb{R}^2$  is a vector of linear coefficients and  $\phi \in \mathbb{R}^3$  is the offset. The set of coefficients  $\theta$  and  $\phi$  that satisfy the rule  $f(\cdot)$  can be derived by solving the following optimization function:

$$\min_{\theta, \phi} \|a_3^q - (A_{1,2}^q \theta + \phi)\|. \quad (9)$$

We could solve the optimization problem by least-squares estimator (LSE) [62], i.e.

$$\begin{aligned} \theta_{\text{LS}} &= (A_{1,2}^{q \top} A_{1,2}^q)^{-1} A_{1,2}^{q \top} a_3^q, \\ \phi &= a_3^q - A_{1,2}^q \theta_{\text{LS}}. \end{aligned} \quad (10)$$

To get the closed-form solution for  $\theta_{\text{LS}}$ ,  $A_{1,2}^{q \top} A_{1,2}^q$  should have full rank to derive the matrix inverse. The rank of *Constant* matrices is always 1, while *Progression*, *Arithmetic* and *Distribute\_Three* matrices have full rank. Thus, the pseudo-inverse is used for *Constant* matrices. We will further provide a mathematical inference of conditions that need to be satisfied for each configuration respectively in the next subsection.

The proposed “2+1” formulation not only better simulates human’s reasoning process, but also is more computationally efficient and more elegant to solve. In contrast, the “8+1” formulation learns a rule  $g_w(\cdot)$  by CNN architectures with weights  $w$  that fulfill:

$$a_{3,3}^q = g_w(a_{1,1}^q, a_{1,2}^q, a_{1,3}^q, a_{2,1}^q, a_{2,2}^q, a_{2,3}^q, a_{3,1}^q, a_{3,2}^q). \quad (11)$$

Compared to the proposed “2+1” formulation, it unnecessarily complicates the RAVEN problems by using a sophisticated formulation and solves it using a much more complicated CNN architecture. One exact reasoning rule can be extracted based on one sample question using the proposed “2+1” formulation,

whereas the “8+1” formulation needs much more samples to derive the rule. In addition, the extracted rules from the “2+1” formulation can be easily interpreted by humans, whereas the “8+1” can not. What’s more, we could reason the correct answer without the help of negative candidate answers using the “2+1” formulation, whereas it is very difficult or even infeasible for the “8+1” formulation.

#### D. Inference of Human-understandable Rules

In this section, we show that the rules inferred from Eqn. (10) can be transferred to a set of human-understandable rules, and the human-understandable rules used in the RAVEN problems such as *Constant*, *Progression*, *Arithmetic* and *Distribute\_Three* can be well represented by the rules derived from Eqn. (10). By deriving and utilizing human-understandable rules, humans could have more insights of the underlying reasoning process and at the time have more confidence on the reliable reasoning outcomes of the model. Take note that when the rules are extracted using Eqn. (10), we do not require any additional prior knowledge on the underlying rules besides the human’s understanding of the rules themselves.

When constructing the RAVEN dataset, Zhang *et al.* [10] considered four types of rules that could be applied row-wisely on the  $3 \times 3$  image matrix: *Constant*, *Progression*, *Arithmetic* and *Distribute\_Three*. Those rules can be defined as follow:

**Definition 1** A question matrix  $A^q$  satisfies *Constant Rule* iff  $a_3^q = a_1^q = a_2^q$ .

**Definition 2** A question matrix  $A^q$  satisfies *Progression Rule* iff  $a_3^q = 2a_2^q - a_1^q$ . Note that  $a_1^q \neq a_2^q$ , otherwise it becomes a *Constant Rule*.

**Definition 3** A question matrix  $A^q$  satisfies *Arithmetic Rule* iff  $a_3^q = a_1^q \pm a_2^q$ .

**Definition 4** A question matrix  $A^q$  satisfies *Distribute\_Three Rule* iff  $a_2^q = S a_1^q$  (observed) and  $a_3^q = S a_2^q$ , where  $S = \begin{bmatrix} 0 & 1 & 0 \\ 0 & 0 & 1 \\ 1 & 0 & 0 \end{bmatrix}$  or  $\begin{bmatrix} 0 & 0 & 1 \\ 1 & 0 & 0 \\ 0 & 1 & 0 \end{bmatrix}$ .

Provided the definitions of rules above, in the rest of the section, we aim to prove that a set of reasoning rules can be obtained using Eqn. (10), which correspond to these four types of human-understandable rules, as outlined in **Theorem 1**.

**Theorem 1** By solving the RAVEN problems using Eqn. (10), 4 general groups of parameterized reasoning functions can be yielded as Eqn. (13), (15), (17) and (19), which correspond to human-understandable rules: *Constant*, *Progression*, *Arithmetic* and *Distribute\_Three* respectively.

To prove **Theorem 1**, we need to prove the sufficient and necessary conditions of four independent groups of reasoning rules as stated in **Lemma 1-4**, which relate to *Constant*, *Progression*, *Arithmetic* and *Distribute\_Three*, respectively.

**Lemma 1** The *Constant Rule* can be equivalently represented as a set of parameterized rules as Eqn. (13) obtained using Eqn. (10).

**Proof.** If  $A^q$  satisfies the *Constant* rule, based on **Definition 1**,

$$A_{1,2}^q = [a_1^q \quad a_1^q], a_3^q = a_1^q. \quad (12)$$

Substitute Eqn. (12) into Eqn. (10), with mentioned matrix pseudo-inverse  $(A_{1,2}^q{}^\top A_{1,2}^q)^\dagger$ , we can get:

$$\begin{aligned} \hat{\theta}_{LS}^C &= (A_{1,2}^q{}^\top A_{1,2}^q)^{-1} A_{1,2}^q{}^\top a_3^q = \begin{bmatrix} 0.5 \\ 0.5 \end{bmatrix}, \\ \hat{\phi}^C &= a_3^q - A_{1,2}^q \hat{\theta}_{LS}^C = 0. \end{aligned}$$

The parameterized function for *Constant Rule* is hence:

$$a_3^q = A_{1,2}^q \cdot \begin{bmatrix} 0.5 \\ 0.5 \end{bmatrix}. \quad (13)$$

It is trivial to prove that given Eqn. (13) and observed  $a_1^q$  and  $a_2^q$ ,  $A^q$  satisfies the *Constant Rule*.  $\square$

**Lemma 2** The *Progression Rule* can be equivalently represented as a set of parameterized rules as Eqn. (15) obtained using Eqn. (10).

**Proof.** If  $A^q$  satisfies the *Progression* rule, based on **Definition 2**,

$$A_{1,2}^q = [a_1^q \quad a_2^q], a_3^q = 2a_2^q - a_1^q. \quad (14)$$

Substitute Eqn. (14) into Eqn. (10), we can get:

$$\begin{aligned} \hat{\theta}_{LS}^P &= (A_{1,2}^q{}^\top A_{1,2}^q)^{-1} A_{1,2}^q{}^\top a_3^q = \begin{bmatrix} -1 \\ 2 \end{bmatrix}, \\ \hat{\phi}^P &= a_3^q - A_{1,2}^q \hat{\theta}_{LS}^P = 0. \end{aligned}$$

The parameterized function for *Progression Rule* is hence:

$$a_3^q = A_{1,2}^q \cdot \begin{bmatrix} -1 \\ 2 \end{bmatrix}. \quad (15)$$

It is trivial to prove that given Eqn. (15),  $A^q$  satisfies the *Progression Rule*.  $\square$

**Lemma 3** The *Arithmetic Rule* can be equivalently represented as a set of parameterized rules as Eqn. (17) obtained using Eqn. (10).

**Proof.** If  $A^q$  satisfies the *Arithmetic* rule, based on **Definition 3**,

$$A_{1,2}^q = [a_1^q \quad a_2^q], a_3^q = a_1^q \pm a_2^q. \quad (16)$$

Substitute Eqn. (16) into Eqn. (10), we can get:

$$\begin{aligned} \hat{\theta}_{LS}^A &= (A_{1,2}^q{}^\top A_{1,2}^q)^{-1} A_{1,2}^q{}^\top a_3^q = \begin{bmatrix} 1 \\ \pm 1 \end{bmatrix}, \\ \hat{\phi}^A &= a_3^q - A_{1,2}^q \hat{\theta}_{LS}^A = 0. \end{aligned}$$

The parameterized function for *Arithmetic Rule* is hence:

$$a_3^q = A_{1,2}^q \cdot \begin{bmatrix} 1 \\ \pm 1 \end{bmatrix}. \quad (17)$$

It is trivial to prove that given Eqn. (17),  $A^q$  satisfies the *Arithmetic Rule*.  $\square$

**Lemma 4** The *Distribute\_Three Rule* can be equivalently represented as a set of parameterized rules as Eqn. (19) obtained using Eqn. (10).

**Proof.** If  $A^q$  satisfies the *Distribute\_Three* rule, based on **Definition 4**,

$$\begin{aligned} A_{1,2}^q &= [a_1^q \quad S a_1^q], a_3^q = S a_2^q = S(S a_1^q), \\ S &= \begin{bmatrix} 0 & 1 & 0 \\ 0 & 0 & 1 \\ 1 & 0 & 0 \end{bmatrix} \text{ or } \begin{bmatrix} 0 & 0 & 1 \\ 1 & 0 & 0 \\ 0 & 1 & 0 \end{bmatrix}. \end{aligned} \quad (18)$$



(a) A panel of question frames at intervals of time extracted from real-world videos for object detection and tracking.



(b) Candidate answer frames extracted from real-world videos. The correct frame is marked in red.

Figure 3. An example of the newly developed RPM-like One-shot Frame-prediction (ROF) dataset used for street scene understanding and video frame prediction. In (a), the three rows represent three different video sequences extracted from the UA-DETRAC dataset [43], and the frames are extracted at a predefined time interval. Based on the reasoning rules learned from the first two rows, the target is to select the proper future frame in the third row based on the spatio-temporal information extracted from the first two frames.

Substitute Eqn. (18) into Eqn. (10), we can get:

$$\begin{aligned}\hat{\theta}_{LS}^D &= (\mathbf{A}_{1,2}^q{}^\top \mathbf{A}_{1,2}^q)^{-1} \mathbf{A}_{1,2}^q{}^\top \mathbf{a}_3^q = \left[ \frac{s}{p+s} \right], \\ \hat{\phi}^D &= \mathbf{a}_3^q - \mathbf{A}_{1,2}^q \hat{\theta}_{LS}^D \\ &= \left( \mathbf{S}^\top - \frac{s}{p+s} (\mathbf{I}_3 + \mathbf{S}) \right) \mathbf{a}_1^q,\end{aligned}$$

where  $p = \mathbf{a}_1^q{}^\top \mathbf{a}_1^q$ ,  $s = \mathbf{a}_1^q{}^\top \mathbf{S} \mathbf{a}_1^q$ . The parameterized function for the *Distribute\_Three* Rule is hence:

$$\mathbf{a}_3^q = \mathbf{A}_{1,2}^q \cdot \left[ \frac{s}{p+s} \right] + \left( \mathbf{S}^\top - \frac{s}{p+s} (\mathbf{I}_3 + \mathbf{S}) \right) \mathbf{a}_1^q. \quad (19)$$

It is trivial to prove that given Eqn. (19),  $\mathbf{A}^q$  satisfies *Distribute\_Three* Rule.  $\square$

#### IV. RPM-LIKE ONE-SHOT FRAME-PREDICTION DATASET

A RPM-like One-shot Frame-prediction (ROF) dataset is constructed to evaluate the proposed method in a practical real-world application. Video frame prediction relies on understanding the spatio-temporal information of historical frames.

Traditionally, a set of previous video frames are needed to predict the next frame [63], while in this paper, the future frame is predicted based on two previous distant frames only.

##### A. Dataset Construction

The ROF dataset is constructed based on the UA-DETRAC dataset for object detection and tracking [43], consisting of 100 challenging videos captured from real-world traffic scenes. The videos are selected from over 10 hours of monitoring videos acquired by a Canon EOS 550D camera at 24 different locations, which represent various traffic patterns and conditions including urban highway, traffic crossings and T-junctions. The UA-DETRAC dataset consists of over 140,000 frames with rich annotations such as illumination, vehicle type, occlusion, truncation ratio, and vehicle bounding boxes.

The ROF dataset is constructed under the RPM framework, i.e., the future frame is predicted based on the two historical frames sampled at an interval of 15 frames, using the underlying reasoning rules learned from the first two groups of frames sampled similarly from other videos. Such a problem formulation is conceptually more challenging than the classical video prediction tasks, as only two historical frames sampled every

15 frames are given. To simplify the question, the target is to select the correct one from the eight possible answers, where in addition to the correct frame, the other seven candidate answers are randomly sampled at least 15 frames away from the correct frame. One sample question is shown in Fig. 3. The developed ROF dataset consists of 3,000 questions for video frame prediction. Each sample consists of 8 question frames and 8 candidate frames. In total, the dataset consists of 48,000 frames. The developed ROF dataset contains visually complex scenes including environmental backgrounds, multiple vehicle objects and street sights.

#### B. Adaptation of Proposed Os-HURS to ROF Dataset

As the image scene of the ROF dataset is much more complicated than that of the common RPM datasets, the perception module of the proposed Os-HURS is adapted to the ROF dataset. First of all, all the moving objects in each of the frames are detected using Mask R-CNN [64], a state-of-the-art object detector. The Mask R-CNN is robust to recognize almost all moving objects in frames, as shown in Fig. III-D(b). However, identifying the same object across frames remains a challenge. To tackle this, the scale invariant feature transform (SIFT) [65] is utilized to match objects across frames, as shown in Fig. III-D(c). After the pair of objects are matched across different frames, the reasoning module is then applied on the derived attributes such as *Position*, *Size* and *Color* of detected objects across frames, to derive the spatio-temporal reasoning rules. Thanks to the proposed two-step formulation, the adaptation on the perception module does not significantly impact the subsequent reasoning module.

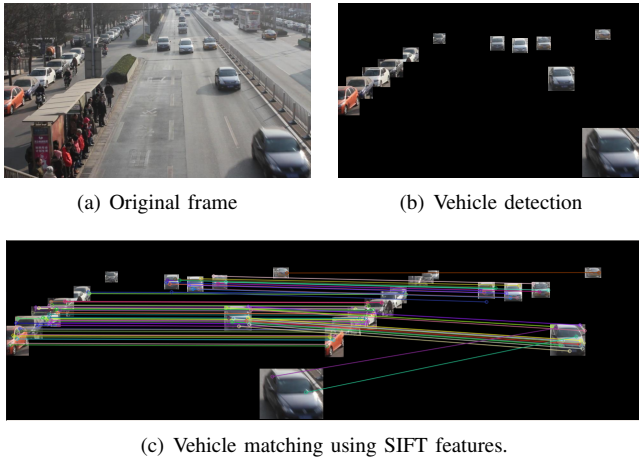


Figure 4. Overview of the perception module of proposed Os-HURS for the ROF dataset. Objects in input frames are firstly detected using Mask R-CNN. After masking off the background, the corresponding pair of objects are matched using SIFT features. Then the derived attributes such as *Position*, *Size* and *Color* of objects can be used in the subsequent logic reasoning.

## V. EXPERIMENTAL RESULTS

Large RPM datasets such as RAVEN and I-RAVEN are used to evaluate the performance of the proposed Os-HURS and other methods. Experiments are also conducted on the shrunk version of the two datasets. Furthermore, the proposed method and state-of-the-art models are evaluated on the developed ROF dataset for visual reasoning on video frame prediction.

### A. Experimental Settings

1) *Datasets*: Two benchmark datasets, RAVEN [10] and I-RAVEN [14] datasets, are used in the experiments. In addition, to show that the proposed method requires much fewer training samples, a portion of training data of RAVEN and I-RAVEN datasets are used whereas other remains the same. These datasets are referred as Shrunk-RAVEN dataset.

**RAVEN**: The size of question sets in the RAVEN dataset [10] is 70,000. The dataset is randomly split into 10 folds, with 6 folds for training, i.e. 42,000 training samples, and 2 folds for validation and 2 folds for testing respectively. Each question contains 8 question images, arranged as a  $3 \times 3$  image matrix with the last one missing, and 8 candidate answers. In the RAVEN dataset, given the first 8 images of the question, the objective is to deduce the reasoning rules from the first 8 images and choose one image from the 8 candidate images as the correct one. The candidate answers are generated by permutation from the ground-truth answer image, and each permuted image is derived by randomly shifting one attribute value. The dataset is equally distributed into 7 problem configurations, i.e. *Center*,  $2 \times 2$  *Grid*,  $3 \times 3$  *Grid*, *Left-Right*, *Up-Down*, *Out-InCenter* and *Out-InGrid*. Each question contains 6 visual attributes (*Angle*, *Number*, *Position*, *Type*, *Size* and *Color*) and 4 underlying rules (*Constant*, *Progression*, *Distribute\_Three* and *Arithmetic*).

Attribute *Angle* is an irrelevant attribute in solving the RPM problem, whereas other attributes may follow one of the underlying reasoning rules. In configuration *Center*, *Left-Right*, *Up-Down* and *Out-InCenter*, attribute *Number* and *Position* are the same for all questions in the same configuration. In configuration  $2 \times 2$  *Grid*,  $3 \times 3$  *Grid* and *Out-InGrid*, either *Number* or *Position* is selected as the underlying construction rule, which implies that the other one becomes an irrelevant attribute, and hence complicates the problem, as misleading rules may be generated from these irrelevant attributes.

Besides irrelevant attributes, Zhang *et al.* [10] mentioned that they introduced extra *noise* information to problem panels as *Uniformity*. It refers to randomly changing portions of entities in question samples. See Fig. 1 for example, the *Color* values vary freely but *Number*, *Type* and *Size* attributes follow the underlying rules. Specifically, the question panel was originally set with *Constant* rule in *Color* attribute, but it was enshadowed with random color values. Therefore, the *Color* attribute may mislead the reasoning process and hence the problem becomes more challenging.

**Impartial-RAVEN (I-RAVEN)**: The original RAVEN dataset may lead to a shortcut that the aggregation of most common values for each attribute could be the correct answer [14]. To address this problem, Hu *et al.* [14] designed an I-RAVEN dataset, by changing the permutation scheme of the candidate answers. Instead of random permutation of one attribute at a time in the RAVEN dataset, the negative candidate answers of the I-RAVEN dataset are generated by hierarchically permuting one attribute of the ground-truth answer in three iterations. In each iteration, two child nodes are generated, where one node remains the same with the parent node and the other permutes one attribute. An example is shown in Fig. 5(b).

Other than this, the same evaluation protocol as in the original RAVEN dataset is used.

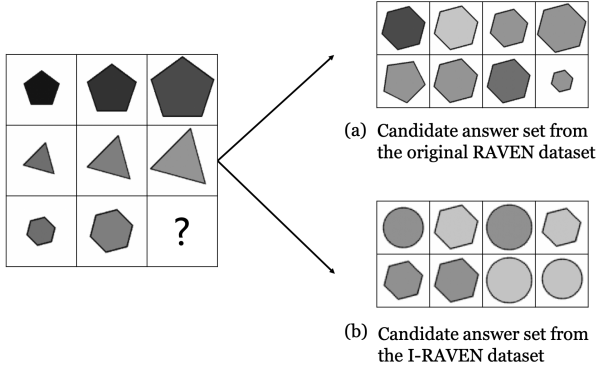


Figure 5. Different candidate answer sets by the RAVEN dataset [10] and the I-RAVEN dataset [14]. One may aggregate the correct answer by selecting the most common attribute from the candidate answers in the original RAVEN dataset, while it is not feasible to do so in the I-RAVEN dataset.

**Shrunk-RAVEN:** One of the major advantages of the proposed approach is that one reasoning rule can be deduced from each sample question, thanks to the proposed two-step framework and “2+1” formulation, while existing approaches need many more samples. The proposed Os-HURS only requires a minimal amount of training samples covering the possible reasoning rules. To verify this, we conduct a series of experiments on shrunk RAVEN-like datasets, where only a portion of the original dataset is randomly selected for training, while the testing samples of the original dataset remain unchanged. As shown later, the proposed approach achieves a competitive performance by utilizing only approximately 1/64 of the original training data. Similar experiments are carried out on both the RAVEN and I-RAVEN datasets.

2) *Compared Methods:* We conduct experiments on the RAVEN [10], I-RAVEN [14] and Shrunk-RAVEN datasets. We use the default image size of  $80 \times 80$ , to avoid unexpected effect of image size to the reasoning accuracy. We compare the proposed method with CNN-based models, which mostly utilize the “8+1” formulation, including LSTM, WReN [11], CNN, ResNet-18 [1], ResNet-18+DRT [10], LEN [37], CoPINet [36] and SRAN [14]. These compared approaches are recently published in reputable journals or conferences. The experimental results are mainly referred from [36] and [14].

**LSTM** Zhang *et al.* [10] extracted image features using a CNN, followed by an LSTM network, and added a two-layer MLP at the end for prediction.

**WReN** Wild Relation Network (WReN) *et al.* [11] utilizes the Relation Network [8] to calculate the probability of each candidate answer to be the correct one.

**CNN** This method contains a four-layer CNN for feature extraction and a two-layer MLP with a softmax layer for prediction, as outlined in [10].

**ResNet-18** The original ResNet-18 is utilized as the feature extractor and a two-layer MLP with a softmax layer is used for prediction, as outlined in [10].

**ResNet-18+DRT** Zhang *et al.* [10] enhanced the original ResNet-18 with a Dynamic Residual Tree (DRT) module,

which takes the features from the lower layers into the leaf nodes of DRT and gradually updates using the ReLU function following the tree structure, with a residual structure to add the original input to form the output.

**LEN** Logic Embedding Network (LEN) developed by Zheng *et al.* [37] assembles the possible candidate answer embeddings to the 8 question panel embeddings, and calculates scores for all possible combinations ( $C_9^3 = 84$ ). The model outputs the predicted answer with the highest score.

**CoPINet** Zhang *et al.* [36] designed Contrastive Perceptual Inference Network (CoPINet), which achieves the previously published best results on the RAVEN dataset. It models the probability of each candidate answer by applying a contrasting module on a perception module, with the question panel and each one of the candidate answers as the input.

**SRAN** Hu *et al.* [14] developed Stratified Rule-Aware Network (SRAN), which achieves the previously published best results on the I-RAVEN dataset. It utilizes a hierarchical rule embedding module and a gated embedding fusion module to output the rule embedding given two row sequence.

## B. Comparisons to State-of-the-art Methods on RPMs

1) *Performance on RAVEN:* The proposed method is compared to various models [8], [10], [36], [37]. The results are summarized in Table I.

We can see from Table I that in *Center*, *Left-Right*, *Up-Down* and *Out-InCenter* configurations, the proposed method achieves almost perfect accuracy. Attributes  $N$  and  $P$  are the same for each configuration, and hence have the minimal disturbance on the reasoning process. Thanks to the proposed two-step framework and “2+1” formulation, one precise rule can be extracted from a question panel for each attribute to form the rule pool, which can help the solver in the testing phase to solve questions based on the derived rule.

Although for *Center*, *Left-Right* and *Out-InCenter* configurations, the proposed method achieves a nearly perfect accuracy, there are still some failure cases. One remaining challenge is that attributes of the first two rows for some testing question panels  $I^{q'}$  are identical so that it is not sufficient to determine any concrete rule, which may lead to failure cases. In  $2 \times 2$  *Grid*,  $3 \times 3$  *Grid* and *Out-InGrid* configurations, the accuracy is relatively low compared to other configurations, which is mainly due to the existence of irrelevant attributes in these configurations. It is difficult to detect irrelevant attributes using one sample question only. CoPINet [36] aggregates the reasoning rules based on a set of samples, which could be the reason why it outperforms the proposed method in the *O-IG* configuration. Other than this configuration, the proposed method consistently and significantly outperforms the previously best performed method, CoPINet, on the RAVEN dataset. On average, the performance gain is 2.2%.

2) *Performance on I-RAVEN:* The proposed method is compared to a variety of models [8], [10], [14], [36], [37]. The results are summarized in Table II. As shown in Table II, the proposed method consistently and significantly outperforms all the compared approaches. It improves the previously published best result by SRAN [14] from 60.8% to 95.9% on average, as shown in Table II.



Table I

THE COMPARISONS OF REASONING ACCURACY ON THE RAVEN DATASET. ALL THE RESULTS FOR OTHER MODELS ARE REFERRED FROM [36]. THE PROPOSED OS-HURS OUTPERFORMS THE PREVIOUSLY PUBLISHED BEST APPROACH, COPINET [36], BY 2.2% ON AVERAGE.

Methods	Acc	Center	2×2 Grid	3×3 Grid	Left-Right	Up-Down	Out-InCenter	Out-InGrid
LSTM	13.1%	13.2%	14.1%	13.7%	12.8%	12.4%	12.2%	13.0%
WReN [11]	34.0%	58.4%	38.9%	37.7%	21.6%	19.7%	38.8%	22.6%
CNN	37.0%	33.6%	30.3%	33.5%	39.4%	41.3%	43.2%	37.5%
ResNet	53.4%	52.8%	41.9%	44.3%	58.8%	60.2%	63.2%	53.1%
ResNet+DRT [10]	59.6%	58.1%	46.5%	50.4%	65.8%	67.1%	69.1%	60.1%
LEN [37]	72.9%	80.2%	57.5%	62.1%	73.5%	81.2%	84.4%	71.5%
CoPINet [36]	91.4%	95.1%	77.5%	78.9%	99.1%	99.7%	98.5%	<b>91.4%</b>
<b>Proposed Os-HURS</b>	<b>93.6%</b>	<b>99.9%</b>	<b>86.0%</b>	<b>80.9%</b>	<b>99.9%</b>	<b>100.0%</b>	<b>99.8%</b>	88.9%

Table II

THE COMPARISONS OF REASONING ACCURACY ON THE I-RAVEN DATASET. THE RESULTS FOR OTHER MODELS ARE REFERRED FROM [14]. THE PROPOSED OS-HURS IMPROVES THE PERFORMANCE OF PREVIOUSLY PUBLISHED BEST METHOD, SRAN [14], FROM 60.8% TO 95.9% ON AVERAGE.

Methods	Acc	Center	2×2 Grid	3×3 Grid	Left-Right	Up-Down	Out-InCenter	Out-InGrid
LSTM	18.9%	26.2%	16.7%	15.1%	14.6%	16.5%	21.9%	21.1%
WReN [11]	23.8%	29.4%	26.8%	23.5%	21.9%	21.4%	22.5%	21.5%
ResNet	40.3%	44.7%	29.3%	27.9%	51.2%	47.4%	46.2%	35.8%
ResNet+DRT [10]	40.4%	46.5%	28.8%	27.3%	50.1%	49.8%	46.0%	34.2%
LEN [37]	41.4%	56.4%	31.7%	29.7%	44.2%	44.2%	52.1%	31.7%
Wild ResNet	44.3%	50.9%	33.1%	30.8%	53.1%	52.6%	50.9%	38.7%
CoPINet [36]	46.1%	54.4%	36.8%	31.9%	51.9%	52.5%	52.2%	42.8%
SRAN [14]	60.8%	78.2%	50.1%	42.4%	70.1%	70.3%	68.2%	46.3%
<b>Proposed Os-HURS</b>	<b>95.9%</b>	<b>100.0%</b>	<b>89.8%</b>	<b>88.3%</b>	<b>99.9%</b>	<b>100.0%</b>	<b>100.0%</b>	<b>93.6%</b>

Table III

THE PROPOSED OS-HURS IS COMPARED WITH PREVIOUSLY BEST PERFORMED METHOD COPINET [36] USING DIFFERENT TRAINING DATASET SIZES ON THE RAVEN DATASET. THE PROPOSED METHOD CONSISTENTLY AND SIGNIFICANTLY OUTPERFORMS COPINET ON ALL SETTINGS.

Training set size		658	1,316	2,625	5,250	10,500	21,000
CoPINet [36]	Center	45.75%	47.50%	57.70%	70.15%	98.20%	98.50%
	2×2 Grid	51.00%	55.90%	65.20%	73.85%	64.15%	78.15%
	3×3 Grid	53.05%	57.65%	63.30%	68.40%	63.05%	72.70%
	Left-Right	56.90%	66.25%	75.90%	88.85%	99.10%	99.50%
	Up-Down	55.20%	63.75%	73.50%	85.80%	96.45%	99.15%
	Out-InCenter	36.30%	53.60%	56.55%	63.30%	85.30%	97.50%
	Out-InGrid	23.15%	42.50%	42.95%	49.50%	66.95%	78.95%
	Average	45.91%	55.31%	62.16%	71.41%	81.89%	89.21%
Os-HURS	Center	90.50%	96.15%	98.45%	99.60%	99.90%	99.90%
	2×2 Grid	77.60%	79.80%	81.55%	82.35%	82.65%	82.90%
	3×3 Grid	71.30%	72.25%	72.75%	73.35%	73.85%	74.30%
	Left-Right	88.20%	97.85%	99.40%	99.85%	99.85%	99.85%
	Up-Down	91.30%	95.90%	99.15%	99.80%	100.00%	100.00%
	Out-InCenter	90.45%	96.85%	98.90%	99.75%	99.75%	99.75%
	Out-InGrid	81.40%	83.20%	84.40%	84.75%	85.00%	86.00%
	Average	84.39%	88.86%	90.66%	91.35%	91.57%	91.82%

In *Center*, *Left-Right*, *Up-Down* and *Out-InCenter* configurations, the proposed method achieves an almost perfect accuracy. Most models suffer from a performance drop transferring between two datasets, even though they might have excellent performance in original RAVEN, e.g. ResNet+DRT (from 59.6% to 40.4%), LEN (from 72.9% to 41.4%) and CoPINet (from 91.4% to 46.1%). One possible reason is that these models might benefit from the mentioned shortcut to the correct answer implicitly, by contrasting attribute information in candidate answers. The proposed method receives consistent improvements compared with the results obtained on the

original RAVEN dataset. The I-RAVEN dataset addresses the problem of the shortcut to the candidate answer in the RAVEN dataset and it is regarded as a more balanced and fair benchmark. At the same time, it shrinks the search space as shown in Fig. 5. For example, there are four different colors and four different sizes for candidate answers of the RAVEN dataset shown in Fig. 5(a), whereas in the I-RAVEN dataset shown in Fig. 5(b), all visual attributes are balanced into 2. Therefore, as a model with a better generalization capability, the proposed method works well on both datasets, and it achieves a much better performance despite the performance

Table IV

THE PROPOSED OS-HURS IS COMPARED WITH PREVIOUSLY BEST PERFORMED METHOD SRAN [14] USING DIFFERENT TRAINING DATASET SIZES ON THE I-RAVEN DATASET. THE PROPOSED METHOD LARGELY OUTPERFORMS SRAN ON ALL SETTINGS.

Training set size		658	1,316	2,625	5,250	10,500	21,000
SRAN [14]	<i>Center</i>	33.20%	38.25%	51.60%	70.05%	56.55%	78.25%
	<i>2×2 Grid</i>	22.20%	22.55%	27.30%	26.10%	36.65%	49.00%
	<i>3×3 Grid</i>	20.00%	19.05%	22.05%	21.30%	30.10%	42.75%
	<i>Left-Right</i>	28.25%	30.65%	38.55%	35.75%	48.15%	51.05%
	<i>Up-Down</i>	28.20%	29.25%	37.80%	34.30%	47.60%	53.05%
	<i>Out-InCenter</i>	24.80%	19.50%	29.50%	29.80%	37.80%	60.65%
	<i>Out-InGrid</i>	19.95%	18.40%	24.90%	24.50%	28.85%	39.50%
	<i>Average</i>	25.22%	25.40%	33.08%	34.58%	40.81%	53.48%
Os-HURS	<i>Center</i>	98.50%	99.60%	99.85%	99.95%	99.95%	99.95%
	<i>2×2 Grid</i>	85.55%	87.65%	88.85%	89.05%	89.20%	89.60%
	<i>3×3 Grid</i>	79.05%	80.60%	81.55%	81.95%	82.30%	83.30%
	<i>Left-Right</i>	89.65%	99.35%	99.35%	99.75%	99.95%	99.95%
	<i>Up-Down</i>	85.70%	92.20%	99.85%	99.85%	100.00%	100.00%
	<i>Out-InCenter</i>	87.70%	98.65%	99.35%	99.90%	99.90%	99.90%
	<i>Out-InGrid</i>	89.55%	90.75%	91.50%	91.80%	91.90%	92.00%
	<i>Average</i>	87.96%	92.69%	94.34%	94.61%	94.74%	94.96%

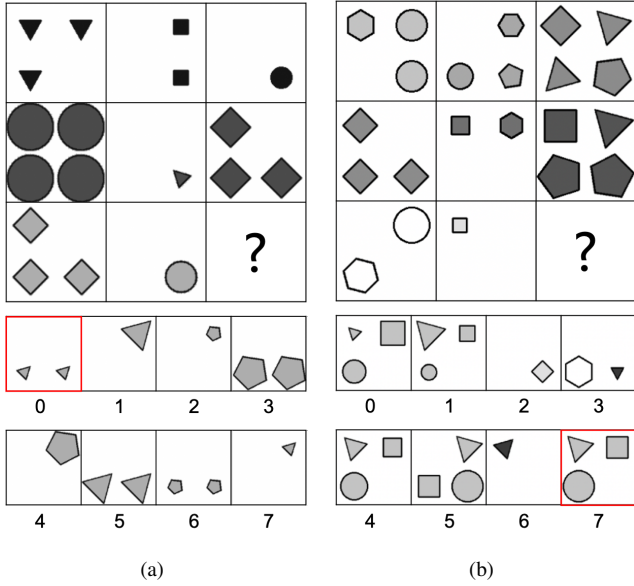
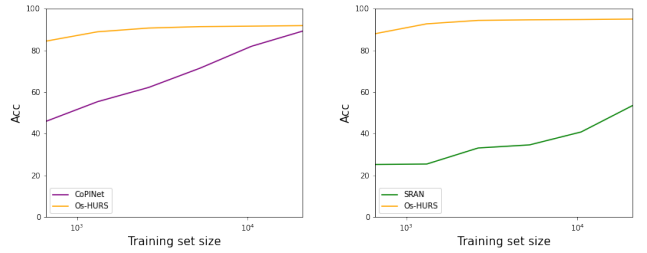


Figure 6. Examples of failure cases of SRAN. (a) SRAN predicts Candidate 7, Os-HURS predicts Candidate 0. (b) SRAN predicts Candidate 5, Os-HURS predicts Candidate 7. Underlying rules: (a) the *Arithmetic* rule on *Number*. (b) the *Arithmetic* rule (addition) on *Position*.

drop by other methods when moving from the original RAVEN dataset to the I-RAVEN dataset.

Existing solution models such as CoPINet and SRAN heavily rely on complex CNN models based on the “8+1” formulation, which unnecessarily complicates the problem so that they may not be able to discover the underlying rules. As shown in Fig. 6(a) as one illustrative example, SRAN makes mistakes on analysis of *Number* attribute, while in the proposed method, because of the proposed “2+1” formulation and the rule inference process, we could predict the correct answer using the discovered underlying reasoning rule, e.g. the *Arithmetic* rule on *Number*.



(a) Overview of the performance on (b) Overview of the performance on  
shrunk RAVEN dataset. shrunk I-RAVEN dataset.

Figure 7. Analysis of influence to performance accuracy by training data size for different models (CoPINet, SRAN, Os-HURS) on the RAVEN dataset and the I-RAVEN dataset.

**3) Performance on Shrunk Datasets:** In this experiment, we evaluate the effect of reducing the training dataset size on the reasoning ability of the model. The proposed Os-HURS is compared with the previously best performed methods, CoPINet [36] on the RAVEN dataset and SRAN [14] on the I-RAVEN dataset, respectively. We use 1/64, 1/32, 1/16, 1/8, 1/4 and 1/2 of the original training dataset, respectively. The results are summarized in Table III and Table IV. For a better view, we also plot the mean accuracy across different configurations for the proposed method and the compared methods on the RAVEN dataset and the I-RAVEN dataset for different sizes of the training dataset, as shown in Fig. 7. The proposed method largely outperforms two compared methods on all settings. Smaller the training dataset size, larger the performance gain.

Our approach is robust even using only 1/64 of the training data. While other methods fail to work, the proposed method still retains a high accuracy. Compared with the proposed method, CoPINet demonstrates a more rapid performance drop when the dataset size decreases, which indicates that it relies on much more training samples than the proposed method. Thanks to the proposed “2+1” formulation that greatly

simplifies the problem, the proposed method could extract one reasoning rule per sample question, and hence requires much few samples to extract a pool of reasoning rules. In addition, the proposed Os-HURS surpasses human-level (84.41% on average [10]) using 658 training samples only.

The experimental results demonstrate the superior reasoning capability of the proposed method over other methods, and the efficiency of the proposed method as one-shot human-understandable ReaSoner.

### C. Comparisons to State-of-the-art Methods on ROF Dataset

The proposed Os-HURS is compared with state-of-the-art methods, CoPINet [36] and SRAN [14], on the developed ROF dataset to analyze the reasoning ability of the models on real-world video frame prediction. The ROF dataset has more complicated image scenes than the RAVEN dataset and its variants. We randomly partition the dataset and utilize half of the dataset as the training set, and the other half as the testing set. The comparison results are shown in Table V.

Table V

THE COMPARISONS OF REASONING ACCURACY ON THE ROF DATASET FOR VIDEO FRAME PREDICTION BETWEEN THE PROPOSED METHOD AND STATE-OF-THE-ART METHODS. THE PROPOSED OS-HURS OUTPERFORMS CoPINet [36] BY 9.24% AND SRAN [14] BY 7.69%.

Models	Reasoning Accuracy
CoPINet [36]	62.34%
SRAN [14]	63.87%
<b>Proposed Os-HURS</b>	<b>71.56%</b>

As shown in Table V, the proposed method significantly outperforms the state-of-the-art models, CoPINet [36] and SRAN [14], on the average reasoning accuracy. The performance gain is 9.24% over CoPINet [36] and 7.69% over SRAN [14]. Thanks to the two-step formulation and “2+1” framework, the proposed method could easily adapt to different visual reasoning scenarios. Also benefited from the proposed efficient and elegant logic reasoning module, the proposed method significantly outperforms the state-of-the-art methods.

For further illustration, we show one example in Fig. 8 that the proposed method works well while CoPINet fails. The example shows that it is indeed difficult to analyze the spatio-temporal relations of objects given only two previous frames at a predefined interval of time, especially when the image scene is complicated, e.g., there are a large number of diversified objects moving in the video sequence. The task will be even challenging when the view angle also changes over time.

## VI. CONCLUSION

In this paper, we introduce an effective solution model to solve RPM problems. Different from the existing black-box CNN-based solution models, we develop a an highly explainable solution model using a two-step framework including the perception module and the reasoning module, to make better use of the developments in both compute vision and logic reasoning societies. With the proposed “2+1” formulation, RPM problems can be solved in a much more elegant and efficient way through the small-scale regression problem

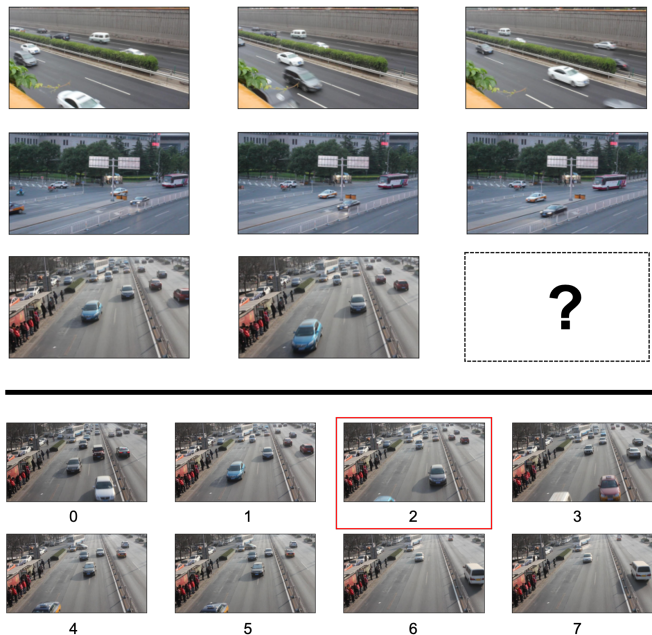


Figure 8. An visual example that the proposed Os-HURS can correctly reason over the complex image scenes, while CoPINet [36] can't. The correct answer is 2 marked in red. Our Os-HURS correctly predicts 2 while CoPINet wrongly predicts 1 as the final answer.

formulation. Finally, the proposed solution could yield human-understandable reasoning rules that previous methods could hardly derive. The ROF dataset is constructed under the RPM framework to evaluate the visual reasoning methods on scene understanding of practical real-world traffic data. A series of experiments are performed on the RAVEN dataset, RAVEN variants and the ROF dataset to evaluate the robustness and generalization of the proposed model. The proposed method outperforms the state-of-the-art models consistently and significantly on all datasets.

## REFERENCES

- [1] K. He, X. Zhang, S. Ren, and J. Sun, “Deep Residual Learning for Image Recognition,” in *Proc. IEEE/CVF Conf. Comput. Vis. Pattern Recognit.*, 2016, pp. 770–778.
- [2] J. Ren, X. Jiang, and J. Yuan, “A Chi-squared-transformed Subspace of LBP Histogram for Visual Recognition,” *IEEE Trans. Image Process.*, vol. 24, no. 6, pp. 1893–1904, 2015.
- [3] S. Ren, K. He, R. Girshick, and J. Sun, “Faster R-CNN: Towards Real-time Object Detection with Region Proposal Networks,” in *Proc. NeurIPS*, 2015, pp. 91–99.
- [4] J. Redmon, S. Divvala, R. Girshick, and A. Farhadi, “You Only Look Once: Unified, Real-time Object Detection,” in *Proc. IEEE/CVF Conf. Comput. Vis. Pattern Recognit.*, 2016, pp. 779–788.
- [5] J. Ren, X. Jiang, J. Yuan, and G. Wang, “Optimizing LBP Structure for Visual Recognition using Binary Quadratic Programming,” *IEEE Signal Process. Lett.*, vol. 21, no. 11, pp. 1346–1350, 2014.
- [6] J. Ren, X. Jiang, J. Yuan, and N. Magnenat-Thalmann, “Sound-event Classification using Robust Texture Features for Robot Hearing,” *IEEE Trans. Multimedia*, vol. 19, no. 3, pp. 447–458, 2016.
- [7] R. Zellers, Y. Bisk, A. Farhadi, and Y. Choi, “From Recognition to Cognition: Visual Commonsense Reasoning,” in *Proc. IEEE/CVF Conf. Comput. Vis. Pattern Recognit.*, 2019, pp. 6720–6731.
- [8] A. Santoro, D. Raposo, D. G. Barrett, M. Malinowski, R. Pascanu, P. Battaglia, and T. Lillicrap, “A Simple Neural Network Module for Relational Reasoning,” in *Proc. NeurIPS*, 2017, pp. 4967–4976.
- [9] N. Messina, G. Amato, F. Carrara, F. Falchi, and C. Gennaro, “Learning Relationship-Aware Visual Features,” in *Proc. Eur. Conf. Comput. Vis.*, 2018.

- [10] C. Zhang, F. Gao, B. Jia, Y. Zhu, and S.-C. Zhu, "RAVEN: A Dataset for Relational and Analogical Visual Reasoning," in *Proc. IEEE/CVF Conf. Comput. Vis. Pattern Recognit.*, 2019.
- [11] A. Santoro, F. Hill, D. Barrett, A. Morcos, and T. Lillicrap, "Measuring Abstract Reasoning in Neural Networks," in *Proc. 35th Int. Conf. Mach. Learn.*, 2018, pp. 4477–4486.
- [12] R. Palm, U. Paquet, and O. Winther, "Recurrent Relational Networks," in *Proc. NeurIPS*, vol. 31, 2018, pp. 3368–3378.
- [13] P. Battaglia, R. Pascanu, M. Lai, D. Jimenez Rezende *et al.*, "Interaction Networks for Learning About Objects, Relations and Physics," in *Proc. NeurIPS*, vol. 29, 2016, pp. 4502–4510.
- [14] S. Hu, Y. Ma, X. Liu, Y. Wei, and S. Bai, "Stratified Rule-Aware Network for Abstract Visual Reasoning," *Proc. 35th AAAI Conf. Artif. Intell.*, vol. 35, no. 2, pp. 1567–1574, 2021.
- [15] L. Wang, Y. Xiong, Z. Wang, Y. Qiao, D. Lin, X. Tang, and L. Van Gool, "Temporal Segment Networks: Towards Good Practices for Deep Action Recognition," in *Proc. Eur. Conf. Comput. Vis.*, 2016, pp. 20–36.
- [16] B. Zhou, A. Andonian, A. Oliva, and A. Torralba, "Temporal Relational Reasoning in Videos," in *Proc. Eur. Conf. Comput. Vis.*, 2018, pp. 803–818.
- [17] J. Lin, C. Gan, and S. Han, "TSM: Temporal Shift Module for Efficient Video Understanding," in *Proc. IEEE/CVF Int. Conf. Comput. Vis.*, 2019, pp. 7083–7093.
- [18] L. Gao, Z. Guo, H. Zhang, X. Xu, and H. T. Shen, "Video Captioning with Attention-Based LSTM and Semantic Consistency," *IEEE Trans. Multimedia*, vol. 19, no. 9, pp. 2045–2055, 2017.
- [19] C. Yan, Y. Tu, X. Wang, Y. Zhang, X. Hao, Y. Zhang, and Q. Dai, "STAT: Spatial-Temporal Attention Mechanism for Video Captioning," *IEEE Trans. Multimedia*, vol. 22, no. 1, pp. 229–241, 2019.
- [20] T. Yao, Y. Pan, Y. Li, and T. Mei, "Exploring Visual Relationship for Image Captioning," in *Proc. Eur. Conf. Comput. Vis.*, 2018, pp. 684–699.
- [21] S. Antol, A. Agrawal, J. Lu, M. Mitchell, D. Batra, C. Lawrence Zitnick, and D. Parikh, "VQA: Visual Question Answering," in *Proc. IEEE/CVF Int. Conf. Comput. Vis.*, 2015, pp. 2425–2433.
- [22] J. Johnson, B. Hariharan, L. Van Der Maaten, F.-F. Li, C. Lawrence Zitnick, and R. Girshick, "CLEVR: A Diagnostic Dataset for Compositional Language and Elementary Visual Reasoning," in *Proc. IEEE/CVF Conf. Comput. Vis. Pattern Recognit.*, 2017, pp. 2901–2910.
- [23] P. Wang, Q. Wu, C. Shen, A. Dick, and A. Van Den Hengel, "FVQA: Fact-Based Visual Question Answering," *IEEE Trans. Pattern Anal. Mach. Intell.*, vol. 40, no. 10, pp. 2413–2427, 2017.
- [24] Y. Zhu, O. Groth, M. Bernstein, and F.-F. Li, "Visual7W: Grounded Question Answering in Images," in *Proc. IEEE/CVF Conf. Comput. Vis. Pattern Recognit.*, 2016, pp. 4995–5004.
- [25] J. Johnson, B. Hariharan, L. Van Der Maaten, J. Hoffman, L. Fei-Fei, C. Lawrence Zitnick, and R. Girshick, "Inferring and Executing Programs for Visual Reasoning," in *Proc. IEEE/CVF Int. Conf. Comput. Vis.*, 2017, pp. 2989–2998.
- [26] J. Zhu, H. Yang, W. Lin, N. Liu, J. Wang, and W. Zhang, "Group Re-identification with Group Context Graph Neural Networks," *IEEE Trans. Multimedia*, 2020, doi: 10.1109/TMM.2020.3013531.
- [27] Z. Wang, T. Chen, J. Ren, W. Yu, H. Cheng, and L. Lin, "Deep Reasoning with Knowledge Graph for Social Relationship Understanding," in *Proc. 27th Int. Joint Conf. Artif. Intell.*, 2018, pp. 1021–1028.
- [28] V. G. Satorras and J. B. Estrach, "Few-Shot Learning with Graph Neural Networks," in *Proc. 6th Int. Conf. Learn. Represent.*, 2018. [Online]. Available: <https://openreview.net/forum?id=BJj6qGbrW>
- [29] J. Reichertz, "Induction, Deduction, Abduction," *The SAGE handbook of qualitative data analysis*, pp. 123–135, 2013.
- [30] D. Krawczyk, *Reasoning: The Neuroscience of How We Think*. Academic Press, 2017.
- [31] J. Raven, "The Raven's Progressive Matrices: Change and Stability over Culture and Time," *Cognitive psychology*, vol. 41, no. 1, pp. 1–48, 2000.
- [32] K. McGregor, M. Kunda, and A. Goel, "Fractals and Ravens," *Artif. Intell.*, vol. 215, pp. 1–23, 2014.
- [33] D. Wang, M. Jamnik, and P. Lio, "Abstract Diagrammatic Reasoning with Multiplex Graph Networks," in *Proc. 8th Int. Conf. Learn. Represent.*, 2020. [Online]. Available: <https://openreview.net/forum?id=ByxQB1BKwH>
- [34] Y. Wu, H. Dong, R. Grosse, and J. Ba, "The Scattering Compositional Learner: Discovering Objects, Attributes, Relationships in Analogical Reasoning," *arXiv preprint arXiv:2007.04212*, 2020.
- [35] Y. Kim, J. Shin, E. Yang, and S. J. Hwang, "Few-shot Visual Reasoning with Meta-analogical Contrastive Learning," in *Proc. NeurIPS*, vol. 33, 2020.
- [36] C. Zhang, B. Jia, F. Gao, Y. Zhu, H. Lu, and S.-C. Zhu, "Learning Perceptual Inference by Contrasting," in *Proc. NeurIPS*, vol. 32, 2019.
- [37] K. Zheng, Z.-J. Zha, and W. Wei, "Abstract Reasoning with Distracting Features," in *Proc. NeurIPS*, 2019, pp. 5842–5853.
- [38] J. An and S. Cho, "Hierarchical Transformer Encoder With Structured Representation for Abstract Reasoning," *IEEE Access*, vol. 8, pp. 200 229–200 236, 2020.
- [39] E. Tjoa and C. Guan, "A Survey on Explainable Artificial Intelligence (XAI): Toward Medical XAI," *IEEE Trans. Neural Netw. Learn. Syst.*, no. 11, pp. 4793–4813, 2020.
- [40] F. B. Abid, M. Sallem, and A. Braham, "Robust Interpretable Deep Learning for Intelligent Fault Diagnosis of Induction Motors," *IEEE Trans. Instrum. Meas.*, vol. 69, no. 6, pp. 3506–3515, 2019.
- [41] R. Srinivasan and A. Chander, "Explanation Perspectives from the Cognitive Sciences—A Survey," in *Proc. 29th Int. Joint Conf. Artif. Intell.*, 7 2020, pp. 4812–4818.
- [42] C. Molnar, "Interpretable Machine Learning: A Guide for Making Black Box Models Explainable," accessed: Nov. 8, 2021. [Online]. Available: <https://christophm.github.io/interpretable-ml-book/>.
- [43] L. Wen, D. Du, Z. Cai, Z. Lei, M.-C. Chang, H. Qi, J. Lim, M.-H. Yang, and S. Lyu, "UA-DETRAC: A New Benchmark and Protocol for Multi-object Detection and Tracking," *Comput. Vis. Image Underst.*, vol. 193, p. 102907, 2020.
- [44] J. Yu, W. Zhang, Y. Lu, Z. Qin, Y. Hu, J. Tan, and Q. Wu, "Reasoning on the Relation: Enhancing Visual Representation for Visual Question Answering and Cross-Modal Retrieval," *IEEE Trans. Multimedia*, vol. 22, no. 12, pp. 3196–3209, 2020.
- [45] H. Zhong, J. Chen, C. Shen, H. Zhang, J. Huang, and X.-S. Hua, "Self-Adaptive Neural Module Transformer for Visual Question Answering," *IEEE Trans. Multimedia*, vol. 23, pp. 1264–1273, 2021.
- [46] F. Liu, J. Liu, Z. Fang, R. Hong, and H. Lu, "Visual Question Answering with Dense Inter-and Intra-modality Interactions," *IEEE Trans. Multimedia*, 2020, doi: 10.1109/TMM.2020.3026892.
- [47] J. Hou, X. Wu, X. Zhang, Y. Qi, Y. Jia, and J. Luo, "Joint Commonsense and Relation Reasoning for Image and Video Captioning," in *Proc. 34th AAAI Conf. Artif. Intell.*, vol. 34, no. 07, 2020, pp. 10 973–10 980.
- [48] Y. Goyal, T. Khot, D. Summers-Stay, D. Batra, and D. Parikh, "Making the V in VQA Matter: Elevating the Role of Image Understanding in Visual Question Answering," in *Proc. IEEE/CVF Conf. Comput. Vis. Pattern Recognit.*, 2017, pp. 6904–6913.
- [49] X. Chen and W. Wang, "Uni-and-Bi-Directional Video Prediction via Learning Object-Centric Transformation," *IEEE Trans. Multimedia*, vol. 22, no. 6, pp. 1591–1604, 2019.
- [50] N.-Y. Kim and J. Kang, "Dynamic Motion Estimation and Evolution Video Prediction Network," *IEEE Trans. Multimedia (Early Access)*, 2020, doi: 10.1109/TMM.2020.3035281.
- [51] S. Oprea, P. Martinez-Gonzalez, A. Garcia-Garcia, J. A. Castro-Vargas, S. Orts-Escobedo, J. Garcia-Rodriguez, and A. Argyros, "A Review on Deep Learning Techniques for Video Prediction," *IEEE Trans. Pattern Anal. Mach. Intell. (Early Access)*, 2020, doi: 10.1109/TPAMI.2020.3045007.
- [52] H. Gammulle, S. Denman, S. Sridharan, and C. Fookes, "Predicting the Future: A Jointly Learnt Model for Action Anticipation," in *Proc. IEEE/CVF Int. Conf. Comput. Vis.*, 2019, pp. 5562–5571.
- [53] O. Makansi, E. Ilg, O. Cicek, and T. Brox, "Overcoming Limitations of Mixture Density Networks: A Sampling and Fitting Framework for Multimodal Future Prediction," in *Proc. IEEE/CVF Conf. Comput. Vis. Pattern Recognit.*, 2019, pp. 7144–7153.
- [54] A. Bhattacharyya, M. Fritz, and B. Schiele, "Long-Term On-Board Prediction of People in Traffic Scenes Under Uncertainty," in *Proc. IEEE/CVF Conf. Comput. Vis. Pattern Recognit.*, 2018, pp. 4194–4202.
- [55] W. Liu, W. Luo, D. Lian, and S. Gao, "Future Frame Prediction for Anomaly Detection—A New Baseline," in *Proc. IEEE/CVF Conf. Comput. Vis. Pattern Recognit.*, 2018, pp. 6536–6545.
- [56] J. Walker, A. Gupta, and M. Hebert, "Dense Optical Flow Prediction from A Static Image," in *Proc. IEEE/CVF Int. Conf. Comput. Vis.*, 2015, pp. 2443–2451.
- [57] C. Finn, I. Goodfellow, and S. Levine, "Unsupervised Learning for Physical Interaction Through Video Prediction," in *Proc. NeurIPS*, vol. 29, 2016, pp. 64–72.
- [58] X. Jia, B. De Brabandere, T. Tuytelaars, and L. V. Gool, "Dynamic Filter Networks," in *Proc. NeurIPS*, vol. 29, 2016, pp. 667–675.
- [59] B. Jin, Y. Hu, Q. Tang, J. Niu, Z. Shi, Y. Han, and X. Li, "Exploring spatial-temporal multi-frequency analysis for high-fidelity and temporal-consistency video prediction," in *2020 IEEE/CVF Conference on Computer Vision and Pattern Recognition (CVPR)*, 2020, pp. 4553–4562.
- [60] R. Villegas, J. Yang, Y. Zou, S. Sohn, X. Lin, and H. Lee, "Learning to Generate Long-Term Future via Hierarchical Prediction," in *Proc. 34th Int. Conf. Mach. Learn.*, 2017, pp. 3560–3569.

- [61] R. Brunelli, *Template Matching Techniques in Computer Vision: Theory and Practice*. John Wiley & Sons, 2009.
- [62] E. G. Larsson and Y. Selén, “Linear Regression with A Sparse Parameter Vector,” *IEEE Trans. Signal Process.*, vol. 55, no. 2, pp. 451–460, 2007.
- [63] W. Byeon, Q. Wang, R. K. Srivastava, and P. Koumoutsakos, “ContextVP: Fully Context-Aware Video Prediction,” in *Proc. Eur. Conf. Comput. Vis.*, 2018, pp. 753–769.
- [64] K. He, G. Gkioxari, P. Dollár, and R. Girshick, “Mask R-CNN,” in *Proc. IEEE/CVF Int. Conf. Comput. Vis.*, 2017, pp. 2961–2969.
- [65] D. G. Lowe, “Distinctive Image Features from Scale-Invariant Key-points,” *Int. J. Comput. Vis.*, vol. 60, no. 2, pp. 91–110, 2004.